2-1605

Assessing and Projecting Greenhouse Gas Release from Large-scale Permafrost Degradation

Kazuyuki SAITO

Japan Agency for Marine-Earth Science and Technology (JAMSTEC)

3173-25 Showa-machi, Kanazawa-ku, Yokohama-city, Kanagawa 236-0001 Japan

E-mail: ksaito@jamstec.go.jp

Permafrost is a large reservoir of frozen soil organic carbon (SOC; about half of all the terrestrial storage). Therefore, its degradation (i.e., thawing) under global warming may lead to a substantial amount of additional greenhouse gas (GHG) release. Past studies have emphasized the release from slow and reversible warming due to subsurface heat conduction (slow release).

Recently, it has been recognized that thermokarst, which is ground subsidence induced by melting of massive ground ice in ice-rich permafrost (called *yedoma*), affects local and regional societies and ecosystems, and can also be another source of GHGs (especially methane). Methane can be released directly from melted ice (direct release), or by decomposition of newly exposed SOC (secondary release) to accelerate large-scale warming beyond the Arctic.

However, earth system modeling is presently limited by insufficient quantitative understanding of a) thermokarst degradation processes, b) the amount and distribution of ground ice and SOC (including trapped GHGs), and c) the geographical distribution of degradation hazards (vulnerability to degradation in terms of additional GHG release), as well as by the absence of the relevant processes implemented in advanced earth system models. Therefore, thermokarst processes and associated GHG releases remain among large sources of uncertainty in present-day climatic and biogeochemical assessments and in future projections, including relative contributions to global warming from slow, direct and secondary releases.

In this project, we aimed to provide observational evidence and numerical estimates to quantitatively assess and project the impacts of GHG release from ice-rich permafrost degradation. We conducted in-situ and remote (e.g., satellite and airborne) observations, lab analysis of sampled ice and soil cores from multiple circumpolar sites (more than 14 sites from Alaska, Siberia and Svalbard), and numerical model development.

We successfully established and validated the Differential SAR Interferometry (DInSAR) technique to detect the distribution and rates of subsidence in the disturbed landscape of a *yedoma* region (Fig. 1). Average subsidence rates were found to be 1-6cm/year for a wildfire scar on Alaska's North Slope, and 0-3cm/year for abandoned farmland in Central Yakutia, Siberia). The gas content in *yedoma* ice is within a small range of 3-4 ml per 100 g ice (except for about 9 ml per 100 g from Stuphallet, Svalbard, suggestive of glacial origin), but methane concentrations showed large intra- and inter-site variations (51 to 14463 ppmv in site averages. Fig. 2).

A conceptual 2-box model to calculate the budget of subsurface water, ice and carbon was developed, and integrated to simulate the changes and distribution of ground ice and SOC for the recent 125 thousand years (from the Last Interglacial to the present). Further, a high-resolution *yedoma* degradation hazard map was produced, incorporating hydrological-topographical information derived from a 1-arc minute digital elevation model (Fig. 3).

By incorporating the above observation-based and model-derived results into a simple evaluation scheme for direct and secondary release mechanisms, GHG release projections and their contribution as a

consequence of the increase in global-average surface air temperature during this century were investigated. In the upper limit case, the total contribution from direct and secondary releases to the temperature increase during this century ranged from 0.23 to 0.26 K (depending on drier or wetter conditions), which compares well to the upper values obtained by previous studies (ca. 0.24 K, see Table 1).
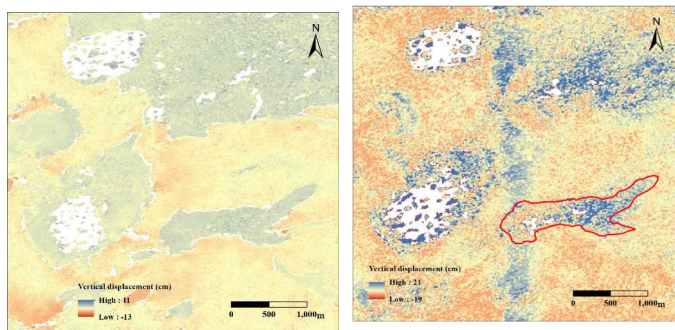
Fig. 1 Surface subsidence after a 2007 wildfire detected by DInSAR (left) of ALOS-PALSAR images on Jul 27, 2009 and Jul 24, 2008, and (right) of ALOS2-PALSAR2 images on Jul 13, 2018 and Jul 17, 2015.
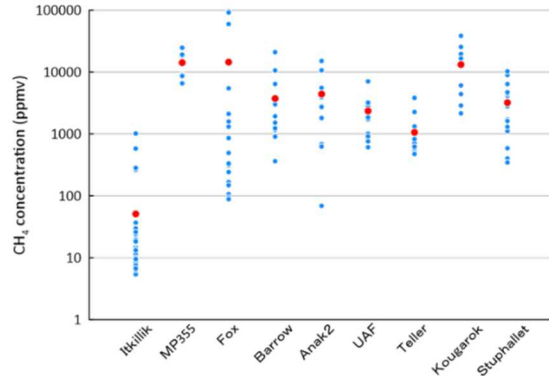
Fig. 2 Distribution of methane concentration in ground-ice bubbles sampled at Alaskan sites. Blue and red dots denote individual and averaged values, respectively.
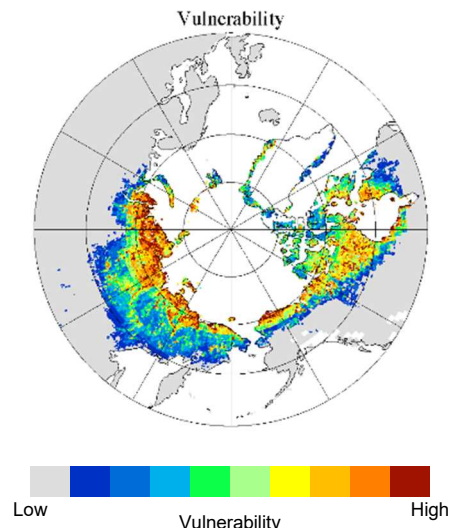
Fig. 3 Map of vulnerability of ice-rich permafrost to degradation.

Table 1 Projection of additional GHG releases induced by permafrost degradation under RCP8.5 warming, and their contribution to global mean surface air temperature increase, and comparison to a previous study (SvD2015, for which dT is expressed by median and 68% range).

Case	CO_2 release [10^3 $TgCO_2$]	CH_4 release [Tg CH_4]	dT [℃]
Dry case	57.84	3943	0.23
Wet case	57.32	6756	0.26
SvD2015	319 (154-517)	1474 (836–2614)	0.09 (0.05–0.14)

Reference:

von Deimling, T. Schneider *et al*. (2015) Observation-based modelling of permafrost carbon fluxes with accounting for deep carbon deposits and thermokarst activity. *Biogeosciences*, 12: 3469-3488.